

# NUMERICAL SIMULATION FOR FLUID-STRUCTURE INTERACTION OF A BLOOD FLOW WITH THE AORTIC VALVE USING THE FEM MONOLITHIC FORMULATION

Truong Sang Ha<sup>1,\*</sup>, Van Chien Vu<sup>1</sup>, Manh Hung Nguyen<sup>1</sup>, Manh Duc Nguyen<sup>1</sup>

<sup>1</sup>*Le Quy Don Technical University, Hanoi, Vietnam*

## Abstract

The paper aims to present a numerical simulation for fluid-structure interaction (FSI) of a blood flow over the aortic valve. The finite element discretization is adopted both for fluid and solid domains. The monolithic scheme is used for the strong coupling of fluid and structure to satisfy kinematic and dynamic equilibrium conditions at the interface. The Navier-Stokes equations of an incompressible flow are solved by using the integrated method based on the ALE formula for the moving grid, and the total Lagrangian formulation is used for the non-linear hyper-elastic material of the aortic valve with the Mooney-Rivlin material model adopted as a constitutive equation for the solid domain. The monolithic FEM method is validated by solving a 3D pressure wave problem and the results are compared to the previous solutions. And then, the present method is employed to investigate blood flow through the aortic valve with a complex geometry. The simulation results can be used for predicting the risk of aortic valve diseases...

**Keywords:** *Fluid-structure interaction; finite element method; aortic valve; monolithic formulation.*

## 1. Introduction

The aortic valve consists of three leaflets that open when the left ventricle of the heart is in the systole phase (contraction) to push out blood to the aorta. The main function of the aortic valve is to close and avoid backflow when the left ventricle is in a rest state (diastole phase). Diseased valves can develop a leak and may have to be replaced [1]. Recently, transcatheter aortic valve (TAV) implantation has been carried out as an alternative to patients with severe aortic stenosis, who are at high risk for surgical therapy. The biomechanical environment of TAV is closely related to the interaction of the motion of the aorta as well as leaflets with the aortic hemodynamics of incompressible flow. Therefore, fluid-structure interaction (FSI) simulation together with an accurate prediction of blood flow is essential. Numerical simulations of FSI for blood vessels such as aortic bifurcation, carotid artery, and aortic valve have received much attention in the last several decades. An accurate simulation of the FSI problems

---

\* Email: sanght.st@lqdtu.edu.vn

plays an important part in the diagnosis and treatment of cardiovascular diseases. However, FSI simulation of a blood flow interacting with an aortic valve remains a challenging problem.

The main challenging problem of FSI for blood flow in the aortic valve comes from the nonlinearity behaviour of fluid and solid domain at the interface. Moreover, the complex geometry of the aortic valve and large deformation of the leaflets also make the FSI problem far more complex. There are numerous studies on the FSI of the blood flow in the aortic valve in literature. Labrosse et al. [1] used a finite element model of a typical human aortic valve with modeling leaflets correction technique. The study aimed to investigate the stress on the valve for the purpose of valve repairing. The FSI of blood flow over the aortic valve is also simulated by Yao et al. [2]. The authors employed the immersed smoothed finite element method with partitioned FSI coupling to investigate the characteristics of unsteady blood flow. Jeannette et al. [3] used the unified continuum Arbitrary Lagrangian-Eulerian (ALE) FEM model to simulate a native valve and a Bileaflet Mechanical Heart Valve in a 3D problem.

In this study, we present a FSI algorithm based on the monolithic algorithm with the full coupling of fluid and structure domain, and the system of FEM discretization is solved simultaneously in one matrix. The rest of the paper is organized as follows: Part 2 gives a brief description of the governing equation of fluid and structure and corresponding FEM formula for the monolithic FSI problem. Part 3 details the numerical solution of a benchmark problem and the aortic valve simulation. Lastly, some conclusions are drawn in Part 4.

## 2. Numerical methods

### 2.1. Governing equations

The blood flow in the vessel wall is assumed as an incompressible flow of a Newtonian fluid, and the governing equations are the incompressible Navier-Stokes equations which can be written as follows in the arbitrary Lagrangian-Eulerian (ALE) framework [4]:

$$\begin{aligned} \nabla \cdot \mathbf{v} &= 0 \quad \text{in } \Omega^f \\ \rho^f \left[ \frac{\partial \mathbf{v}}{\partial t} + (\mathbf{v} - \mathbf{v}^m) \cdot \nabla \mathbf{v} \right] &= \nabla \cdot \boldsymbol{\sigma}^f \quad \text{in } \Omega^f \end{aligned} \quad (1)$$

where  $\rho^f$ ,  $\mathbf{v}$ ,  $\mathbf{v}^m$  and  $\boldsymbol{\sigma}^f$  denote the fluid density, the fluid velocity, the grid velocity, and the fluid stress tensor, respectively. The body force is neglected in present work.

Fluid domain and its boundary are denoted by  $\Omega^f, \Gamma^f$ . The corresponding constitutive equations for fluid flow in Eq. (1) are written as follows:

$$\begin{aligned}\boldsymbol{\sigma}^f &= -p\mathbf{I} + \boldsymbol{\tau}, \\ \boldsymbol{\tau} &= \mu[\nabla\mathbf{v} + (\nabla\mathbf{v})^T]\end{aligned}\quad (2)$$

where  $p, \mu, \boldsymbol{\tau}, \mathbf{I}$  and  $T$  indicate the pressure, the fluid dynamic viscosity, the shear stress tensor, the second-order identity tensor, and the transposition, respectively. The boundary conditions are described as follows:

$$\begin{aligned}\mathbf{v} &= \bar{\mathbf{v}} \text{ on } \Gamma_v^f, \\ \boldsymbol{\sigma}^f \cdot \mathbf{n}^f &= \bar{\mathbf{t}}^f \text{ on } \Gamma_t^f\end{aligned}\quad (3)$$

where  $\mathbf{n}^f$  denotes the outward unit normal vector to the fluid boundary,  $\Gamma_v^f$  and  $\Gamma_t^f$  are the boundaries on which the velocity ( $\bar{\mathbf{v}}$ ) and traction ( $\bar{\mathbf{t}}^f$ ) are imposed on the Dirichlet and Neumann boundary conditions, respectively. The governing equation for solid domain in the Lagrangian framework is written as follows:

$$\rho^s \frac{\partial^2 \mathbf{u}}{\partial t^2} = \nabla \cdot \boldsymbol{\sigma}^s \text{ in } \Omega^s \quad (4)$$

with boundary conditions:

$$\begin{aligned}\mathbf{u} &= \bar{\mathbf{u}} \text{ on } \Gamma_u^f, \\ \boldsymbol{\sigma}^s \cdot \mathbf{n}^s &= \bar{\mathbf{t}}^s \text{ on } \Gamma_t^s\end{aligned}\quad (5)$$

where  $\rho^s, \mathbf{u}$  and  $\boldsymbol{\sigma}^s$  denote the solid density, the displacement of solid, and the solid stress tensor, respectively. The solid domain is denoted by  $\Omega^s$  with a boundary  $\Gamma^s$ .

The constitutive equation of the solid domain is written as follows [5]:

$$\boldsymbol{\sigma}^s = J^{-1} \mathbf{F} \mathbf{S} \mathbf{F}^T; \quad \mathbf{T} = \mathbf{S} \mathbf{F}^T; \quad \mathbf{S} = \mathbf{C} : \mathbf{E}, \quad (6)$$

where  $\mathbf{C}$  denotes a fourth-order tensor representing the material behavior.  $\mathbf{T}$  and  $\mathbf{S}$  are the first and second Piola-Kirchhoff stress tensor, respectively, and  $\mathbf{F}$  and  $J$  denote the deformation gradient tensor and its Jacobian.  $\mathbf{C}$  can be a linear or nonlinear (Mooney-Rivlin) model. More detailed description of the constitutive equation is described in [4].

Let  $\Gamma^{f/s}$  be the interface between the fluid/structure domains (F/S interface). For non-slip condition, both the velocity and traction of fluid domain are equilibrium with

those of the solid at the F/S interface. The two conditions are described by the following formula:

$$\begin{aligned} \mathbf{v} &= \frac{\partial \mathbf{u}}{\partial t} \quad \text{on } \Gamma^{f/s} \\ \boldsymbol{\sigma}^f \cdot \mathbf{n}^f + \boldsymbol{\sigma}^s \cdot \mathbf{n}^s &= 0 \quad \text{on } \Gamma^{f/s} \end{aligned} \quad (7)$$

### 2.2. Finite element formulation for monolithic FSI coupling

The integrated formulation in which the pressure and velocity of fluid flow are solved simultaneously in one system is adopted in this work. The pressure/velocity variable is linearly/quadratically interpolated in a finite element. Fig. 1 shows a *P2P1* finite element for the fluid domain (tetrahedral grid), where the pressure variable is allocated on the vertices and the velocity variables are on both vertices and mid-nodes. Finite element formulation of the governing equation for unsteady incompressible fluid flow is written as follows [4, 6, 7]:

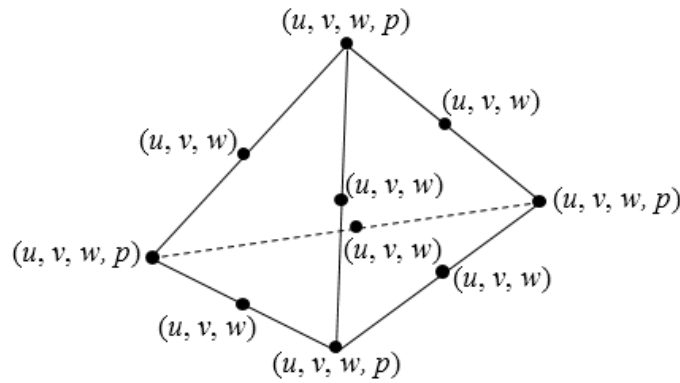


Fig. 1. Degrees of freedom assigned for the *P2P1* finite element

Find  $\mathbf{v} \in H_h^1(\Omega)$ ,  $p \in L_h^2(\Omega)$ , such that

$$\begin{aligned} \int_{\Omega^f} q \nabla \cdot \mathbf{v} d\Omega &= 0 \\ \int_{\Omega^f} \left\{ \mathbf{w} \cdot \rho^f \left[ \frac{\partial \mathbf{v}}{\partial t} + (\mathbf{v} - \mathbf{v}^m) \cdot \nabla \mathbf{v} + \nabla \mathbf{w} : \boldsymbol{\sigma}^f \right] \right\} d\Omega &= \int_{\Gamma^f} [\mathbf{w} \cdot (\boldsymbol{\sigma}^f \cdot \mathbf{n}^f)] d\Gamma \end{aligned} \quad (8)$$

for all admissible functions  $\mathbf{w} \in V_h$ ,  $q \in P_h$ , where

$$V_h = \left\{ \mathbf{w} \mid \mathbf{w} \in H_h^1(\Omega), \mathbf{w} = 0 \text{ on } \Gamma_v^f \right\}, P_h = \left\{ q \mid q \in L_h^2(\Omega) \right\}.$$

The generalised- $\alpha$  method [8] is adopted for an implicit temporal discretization, and the Newmark approximation is employed to obtain the acceleration of fluid from velocity variables:

$$\dot{\mathbf{v}}^{n+1} = \frac{1}{\gamma \Delta t} [\mathbf{v}^{n+1} - \mathbf{v}^n] - \frac{1-\gamma}{\gamma} \dot{\mathbf{v}}^n \quad (9)$$

where  $\mathbf{v}^n$  and  $\gamma$  denote the velocity of fluid flow at  $n^{\text{th}}$  time-step and the coefficient of the the generalised- $\alpha$  method, respectively.

In a solid domain, the displacement variable is quadratically interpolated in an unstructured finite element. Its formulations for the solid domain are written as follows [4]:

Find  $\mathbf{u} \in H_h^1(\Omega)$ , such that

$$\int_{\Omega_0^s} \left[ \mathbf{w} \cdot \rho_0^s \frac{\partial^2 \mathbf{u}}{\partial t^2} + \nabla \mathbf{w} : \mathbf{T} \right] d\Omega = \int_{\Gamma_0^s} [\mathbf{w} \cdot (\mathbf{T} \cdot \mathbf{n}_0^s)] d\Gamma \quad (10)$$

for all admissible functions  $\mathbf{w} \in V_h$ , where

$$V_h = \left\{ \mathbf{w} \mid \mathbf{w} \in H_h^1(\Omega), \mathbf{w} = 0 \text{ on } \Gamma_u^s \right\}.$$

The generalized- $\alpha$  method is also adopted for a solid domain, and the Newmark method - used to compute the acceleration and the displacement of solid from the velocity variable [4].

The strong coupling of fluid and structure equations is accomplished based on the ALE framework in present work. For the monolithic algorithm, velocity variables are shared at the fluid-structure interface so that the kinematic constraint is satisfied automatically by sharing the velocity field at the interface. Summation of fluid and structure equations at the interface cancel out the stress terms of both sides, satisfying the equilibrium constraint. Therefore, the system of FEM discretization for the monolithic coupling FSI problem is shown as follows:

$$\begin{aligned} [\bar{\mathbf{G}}^f] \mathbf{v}^f + [\mathbf{H}^f] (p^f) + [\bar{\mathbf{G}}^s] \mathbf{v}^s &= \mathbf{P}^f + \mathbf{P}^s, \\ [\mathbf{H}^f]^T (\mathbf{v}^f) &= 0 \end{aligned} \quad (11)$$

Or in the matric form:

$$\begin{bmatrix} \bar{\mathbf{G}} & \mathbf{H}^f \\ (\mathbf{H}^f)^T & 0 \end{bmatrix} \begin{bmatrix} \bar{\mathbf{v}} \\ p \end{bmatrix} = \begin{bmatrix} \mathbf{P}^f + \mathbf{P}^s \\ 0 \end{bmatrix} \quad (12)$$

where  $\bar{\mathbf{v}}$  denotes velocity filed for both fluid and solid domain, and  $\bar{\mathbf{G}}$  is general stiffness calculated for the whole simulation;  $\bar{\mathbf{G}}^f$  and  $\mathbf{H}^f$  are the stiffness matrices of velocity and pressure variables of fluid flow are constructed by FEM descretization, respectively. (The details of these matrices and force vectors  $\mathbf{P}^f$ ,  $\mathbf{P}^s$  are discussed in [6, 7]). In the monolithic approach, the velocity variables of both fluid and solid domain

as well as the pressure of fluid flow are obtained together by solving the system (12) in each time-step.

### 2.3. Flow characteristics calculation

In order to investigate the blood flow through the aortic valve, some flow characteristics are measured. The Wall Shear Stress (WSS) and Oscillating Shear Index (OSI) are calculated in this work. The WSS is the shear stress in the layer of fluid next to the wall of a pipe. The WSS components are calculated by [9]:

$$\tau_w = \mathbf{t} - (\mathbf{t} \cdot \mathbf{n})\mathbf{n}, \quad (13)$$

and the traction vector of the surface,  $\mathbf{t}$ , is defined as  $\mathbf{t} = \boldsymbol{\sigma} \cdot \mathbf{n}$ . The WSS is an important quantity for the prediction of hemodynamic disorders. The low WSS region appears to be at high risk of atherogenesis because the stationary blood flow causes the deformation of atheroprotective endothelial cells. The time-averaged WSS is also one of the risk factors for atherogenesis and is defined as:

$$\tau_{w,mean} = \left| \frac{1}{T} \int_0^T \tau_w dt \right|, \quad (14)$$

where  $T$  is one cardiac period. The OSI indicates the degree of the cyclic departure of the WSS vector and is defined by a ratio of the mean WSS and the absolute WSS:

$$OSI = \frac{1}{2} \left( 1 - \frac{\tau_{w,mean}}{\tau_{w,abs}} \right), \quad (15)$$

where the absolute WSS is defined by:

$$\tau_{w,abs} = \frac{1}{T} \int_0^T |\tau_w| dt. \quad (16)$$

The OSI is a measure of the WSS considering acting direction on the endothelial cell during a cycle. A high OSI means that the magnitude of the WSS with opposite direction from its averaged direction is large whereas the low OSI indicates small magnitude of the WSS with opposite direction [9].

## 3. Results and discussions

In this section, the accuracy of the monolithic FEM method was confirmed by comparing with the previous studies. And then, the present method was employed to simulation the blood flow interacting with an aortic valve. The program was written in the FORTRAN language on a single-core machine of a desktop. The mesh smoothing is required for each time step because of the large deformation of the wall. A Laplace equation was solved with a Dirichlet boundary condition at the interface for smoothing

mesh [4], and a remeshing procedure was used whenever the skewness of element is bigger than 0.9 (see Section 3.2). As discussed in [4], although a brick element is known to provide a more accurate solution than the tetrahedral element (especially for the case of hyperelastic materials), a tetrahedral element is used in this study because of easier mesh generation for complex geometry (the aortic valve). From our experience, a second order is required for the tetrahedral element ( $P2$ ) of the solid domain to get an accurate solution. It is also noted that the present method can be implemented on the brick element without any additional complexity.

### 3.1. 3D flow in a straight flexible tube

The first simulation is a pressure wave propagation of incompressible fluid in a 3D flexible tube. The problem was reported in the previous works [4, 10] and has been employed for validation of the present monolithic FEM code. The schematic is shown in Fig. 2, and the dimensions and the material property of the simulation domain are illustrated in Table 1. Both fluid and solid are initially at rest and the tube is fixed in all directions at the two ends. A pressure  $p_{in}$  is set at the inlet of the tube depending on the time simulation as follows:

$$p_{in}(t) = \begin{cases} 1333.2 \text{ Pa} & t \leq 3 \times 10^{-3} \text{ s}; \\ 0 & \text{Pa} \quad t > 3 \times 10^{-3} \text{ s}. \end{cases} \quad (17)$$

Table 1. Dimensions of the simulation domain and material property

Parameter	Symbol	Value
Tube length	$L$	5.0 cm
Tube diameter	$D$	1.0 cm
Wall thickness	$\delta$	0.1 cm
Fluid density	$\rho^f$	1.0 g/cm <sup>3</sup>
Solid density	$\rho^s$	1.2 g/cm <sup>3</sup>
Dynamic viscosity	$\mu$	0.03 Poise
Young's modulus of solid	$E$	$3 \times 10^5$ Pa
Poisson ratio	$\nu$	0.3

At the outlet of the tube, a zero-pressure boundary condition is set for the whole simulation. A  $P2P1$  tetrahedral mesh is used for both fluid and solid domains as shown in Fig. 3. The meshes were generated by using software ICEM/ANSYS with the skewness of element is controlled to be less than 0.5 for both domains. The numbers of elements of fluid and solid are 28,800 and 19,200, respectively. Time step size  $\Delta t$  was

set to  $10^{-4}$  s in this benchmark, the relative error of the nonlinear treatment by Newton-Raphson approach was set to  $10^{-4}$ . The simulation was done for 100 time-steps and the solution was obtained after approximately half an hour.

The pressure contours in the F/S interface with different time instants are shown in Fig. 4, in which the wall deformation is enhanced by a factor of 10 for clarity. The deformation of the tube in the radiation director is approximately around 2% of the diameter. The results obtained from the present monolithic FEM method are in a good agreement with those provided in [10]. Fig. 5 plots the evolution of movement (axial and radiation displacement) at the centre point of the inner tube wall (point M in Fig. 2) for a quantitative comparison. It can be seen that the present results agree well with those obtained by Eken and Sahin [10]. A difference of less than 1% may be due to insufficient mesh resolution.

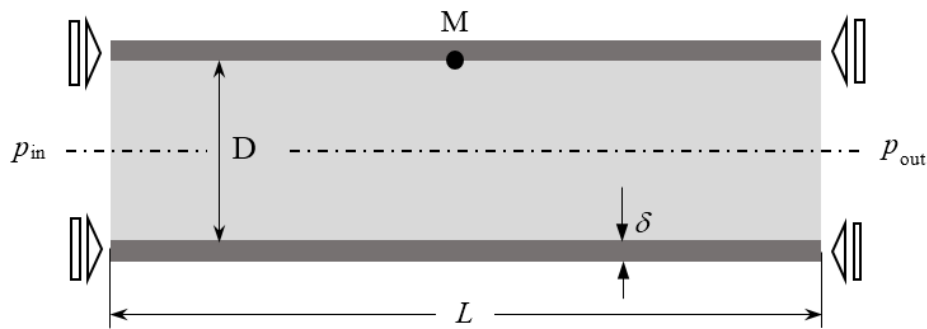


Fig. 2. Schematic of flow in a straight flexible tube [4]

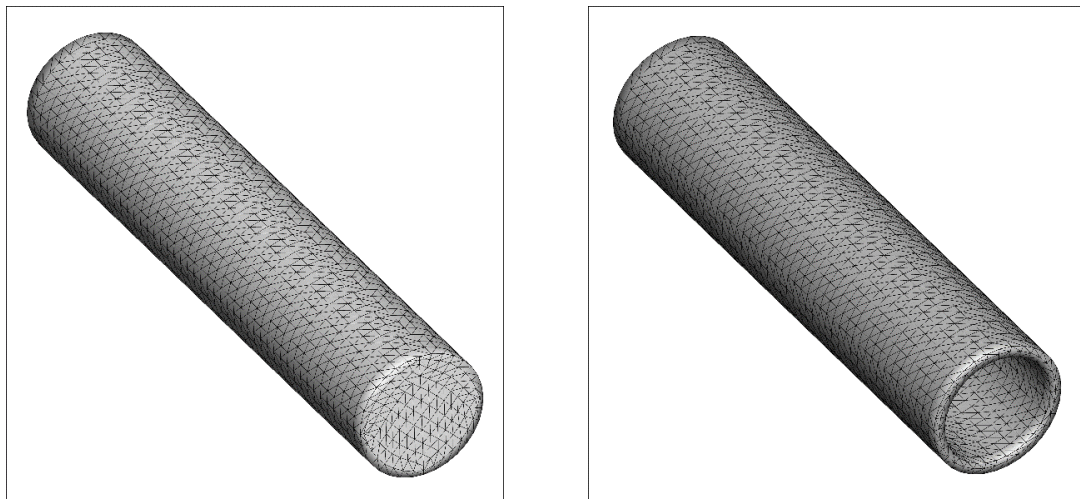


Fig. 3. Grid of fluid and solid domains

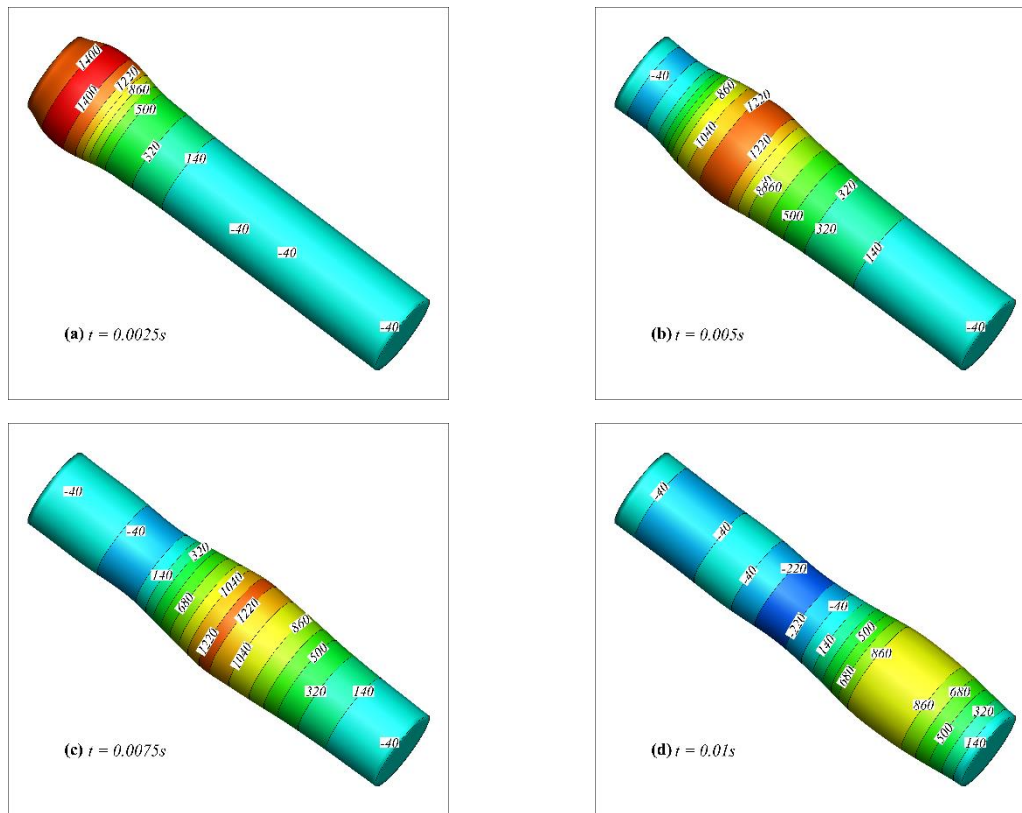
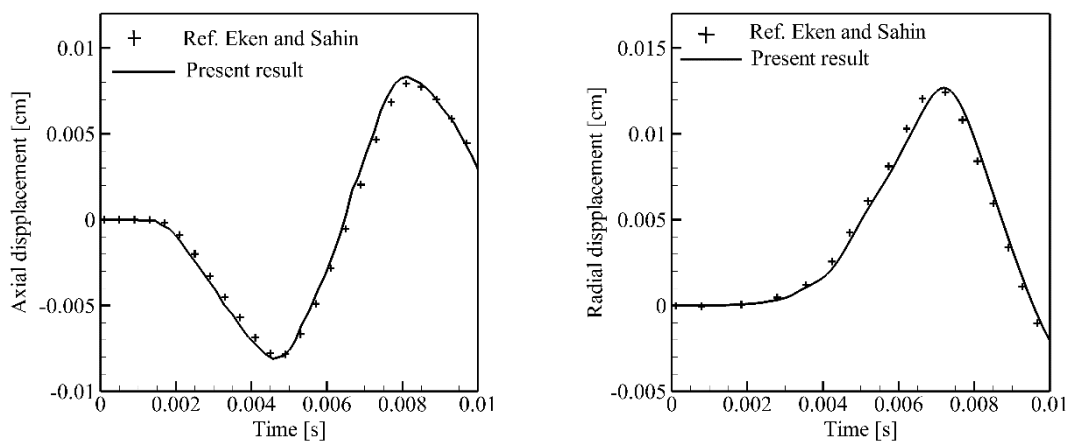


Fig. 4. Pressure contours on the fluid-structure interface at different time  
(The wall deformations were enhanced by a factor of 10 for clarity)



(a) Axial displacement

(b) Radial displacement

Fig. 5. Comparison of the movement of point M obtained from present work  
and results by Eken and Sahin [10]

### 3.2. Blood flow through the aortic valve

In this section, the monolithic FEM is applied for simulation a pulsatile blood flow interacting with an aortic valve. Because we are interested only in the motion of the valve interacting with blood flow, the aortic artery is assumed as a rigid wall with a simple shape. The aortic domain and the valve are chosen from the model in [11]. ANSA software was used to generate meshes on the faces and Tgrid/ICEM was used to generate volume meshes based on meshes on the faces. The skewness of the mesh is less than 0.7 at initial for both domains and a remeshing procedure will be conducted whenever the skewness is bigger than 0.9. Fig. 6 shows the geometry of the valve inside an aortic artery and the corresponding tetrahedral mesh for fluid and solid domains. The numbers of elements at initial are 111,426 and 16,763 for fluid and solid domains, respectively. The boundary condition for the inlet is a pulsatile flow rate as shown in Fig. 7 for one period of  $T = 1.1$  s. At the end of systole ( $\sim 0.35T$ ), the direction of the inflow is inverted to create a backflow that is physiologically consistent and helps the valve close. Diastole starts when the valve is closed and the inflow is set to zero (see Fig. 7). A zero-pressure is set at the outlet [3]. The blood density and dynamic viscosity are given  $\rho^f = 1.05 \text{ g/cm}^3$  and  $\mu = 0.004 \text{ Pa}\cdot\text{s}$  as provided in [12]. The density of the aortic valve is set of  $\rho_0^s = 1.0 \text{ g/cm}^3$  at the reference configuration. The stress-strain relation of the aortic valves is assumed as the Mooney-Rivlin model with the material parameters are given in [13, 14]. The present code was firstly validated for Mooney-Rivlin model in a simple geometry of a beam under a unit tension as described in [15]. Fig. 8 shows the benchmark problem and the comparison of displacement of beam at the end is listed in Table 2. The present results are in a good agreement with those provided in [15] for the Mooney-Rivlin model of solid domain.

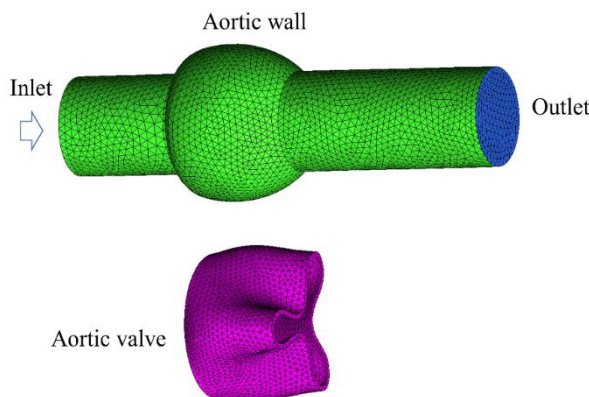


Fig. 6. The geometry and mesh generation of valve inside an aortic artery [11]

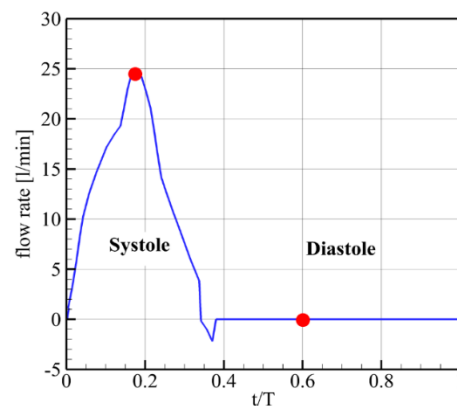
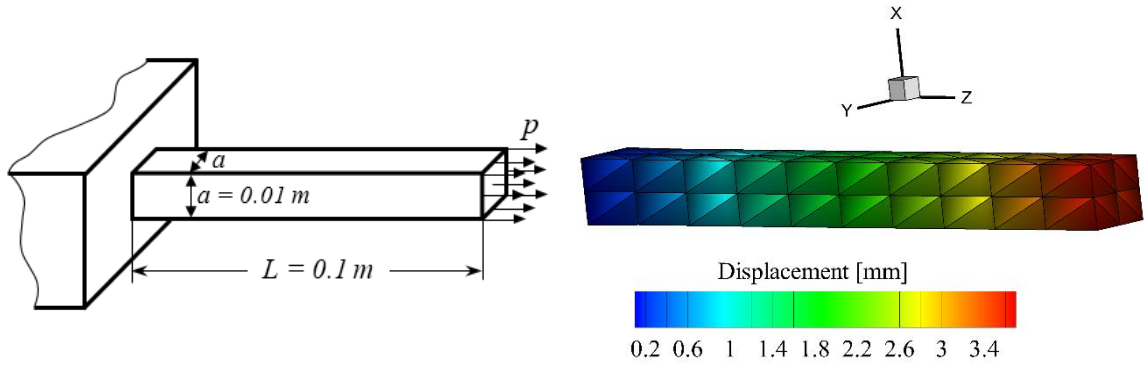


Fig. 7. Flow rate at the inlet of aortic valve [3]



a) Schematic of benchmark problem [15]      b) Displacement of beam with tension of 40 kPa

Fig. 8. A beam loaded by unit tension for validation Mooney-Rivlin model

Table 2. Comparison of displacement of beam at the end (mm)

Tension $p$ , kPa	Reference [15]	Present code
5	0.5	0.5
10	0.95	0.96
40	3.55	3.6

Now the code is employed for simulation of the aortic valve, and the time step size  $\Delta t$  was set to  $5 \times 10^{-5}$  s to get an accurate solution. The simulation results of one period ( $T$ ) were obtained after one week by using a desktop machine (single-core). We only consider the two major phases, systole (valve opened) and diastole (valve closed), and numerical results are examined at the two different instants:  $t_1 = 0.18T$  and  $t_2 = 0.6T$ . The deformations of the valve at the two instants are illustrated in Fig. 9. The valve is fully opened at the systolic phase (Fig. 9a), where the flow rate reaches the maximum value ( $\sim 25$  l/min). The valve is closed when the flow rate is zero at the diastolic phase (Fig. 9b). Fig. 10 shows the streamlines of blood flow through the valve at the two instants. Blood velocity reaches the maximum value ( $\sim 1.4$  m/s) at the peak flow-rate ( $t_1 = 0.18T$ ) of the systole and then decreased to  $\sim 0.3$  m/s at the diastole ( $t_2 = 0.6T$ ). Some vortices appear in the region between the aortic wall and the valve at the systolic phase (Fig. 10a), and backflow is found with many vortices in the aortic artery at the diastolic phase (Fig. 10b). According to the flow through the valve, there is a rapid increase in WSS on the inner wall of the valve at the peak flow-rate as shown in Fig. 11. WSS is then decreased as the flow-rate goes to zero when the valve is closed ( $t_2 = 0.6T$ ). Fig. 12 shows that the OSI value is higher near the edge of the valve.

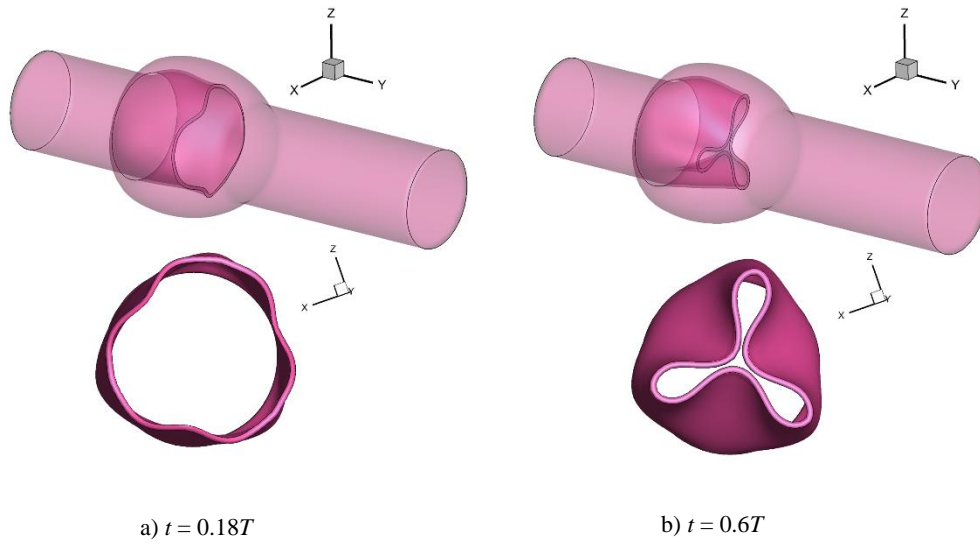


Fig. 9. Deformation of aortic valve at systolic phase (a) and diastolic phase (b)

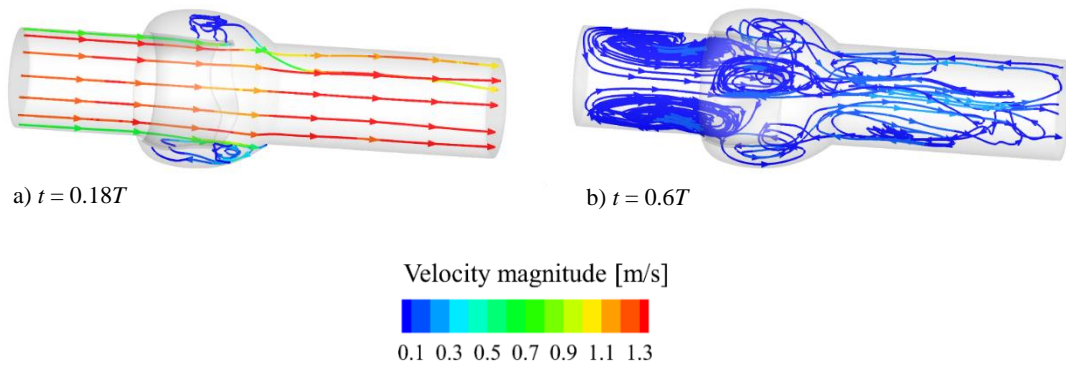


Fig. 10. Streamlines of blood flow through aortic valve at systolic phase (a) and diastolic phase (b)

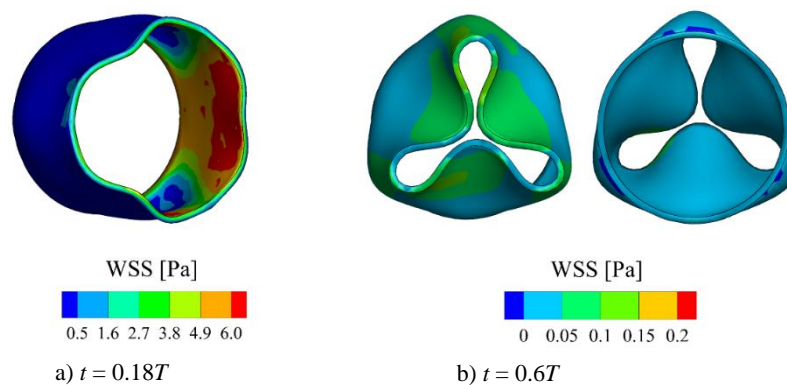


Fig. 11. WSS distribution on the aortic valve at systolic phase (a) and diastolic phase (b)

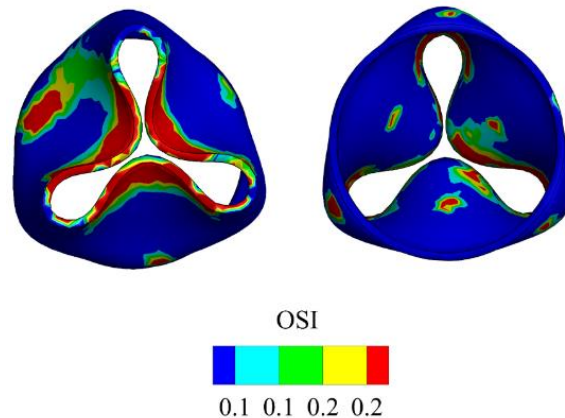


Fig. 12. OSI distribution

#### 4. Conclusion

In this paper, we solve the FSI problem of unsteady blood flow over the aortic valve. The monolithic is used for the FSI coupling of an incompressible fluid with a large displacement of the solid wall. The Mooney-Rivlin model is adopted for the material of the valve to improve the accuracy of the simulation. A  $P2P1$  tetrahedral grid is employed for finite element discretization of the 3D domain. The method is validated by solving the pressure wave in a 3D straight tube. The solution obtained by the present approach is in a good agreement with the previous studies. The simulation results show that the aortic valve is fully opened at the systolic phase corresponding with the maximum flow rate through the valve. At this phase, the peak-flow rate is achieved at time  $0.18T$  with a maximum of wall shear stress (WSS). At the diastolic phase ( $0.6T$ ), the backflow is found with many vortices in the aortic artery. For the whole period, the WSS at the inside of the leaflets is found to be bigger than that at the outside, and the OSI value is higher near the edge of the valve. The flow characteristics may be strongly affected by the geometry of individual aortic valve, therefore, in the future, the patient specific models will be considered to improve the accuracy for predicting the risk of aortic valve diseases.

#### References

- [1] M.R. Labrosse, M. Boodhwani, B. Sohmer, C.J. Beller, "Modeling leaflet correction techniques in aortic valve repair: A finite element study," *Journal of biomechanics*, 44(12), pp. 2292-2298, 2011.
- [2] J. Yao, G.R. Liu, D.A. Narmoneva, R.B. Hinton, Z.Q. Zhang, "Immersed smoothed finite element method for fluid-structure interaction simulation of aortic valves," *Computational Mechanics*, 50(6), pp. 789-804, 2012.

- [3] H.S. Jeannette, J. Johan, J. Niclas, H. Johan, "3D Fluid-Structure Interaction Simulation of Aortic Valves Using a Unified Continuum ALE FEM Model," *Frontiers in Physiology*, (9): 363, 2018.
- [4] S.T. Ha, H.G. Choi, "Investigation on the effect of density ratio on the convergence behavior of partitioned method for fluid–structure interaction simulation," *Journal of Fluids and Structures*, 96, 103050, 2020.
- [5] G.A. Holzapfel, "Nonlinear solid mechanics: A continuum approach for engineering science," *Meccanica*, 2002.
- [6] S.T. Ha, L.C. Ngo, M. Saeed, B.J. Jeon, H.G. Choi, "A comparative study between partitioned and monolithic methods for the problems with 3D fluid–structure interaction of blood vessels," *J. Mech. Sci. Technol.*, 31, pp. 281-287, 2017.
- [7] S. Kang, H.G. Choi, J.Y. Yoo, "Investigation of fluid–structure interactions using a velocity-linked P2/P1 finite element method and the generalized- $\alpha$  method," *Internat. J. Numer. Methods Engrg.*, 90, pp. 1529-1548, 2012.
- [8] J. Chung, G.M. Hu, "A time integration algorithm for structural dynamics with improved numerical dissipation: The generalized- $\alpha$  method," *J. Appl. Mech.*, 60, pp. 371-375, 1993.
- [9] S.H. Lee, "Numerical Simulation of Blood Flow in Flexible Carotid Artery Bifurcation," Ph.D. dissertation, SeoulTech., 2012.
- [10] A. Eken and M. Sahin, "A parallel monolithic algorithm for the numerical simulation of large-scale fluid structure interaction problems," *Int. J. Numer. Methods Fluids*, pp. 687–714, 2016.
- [11] S.T. Ha, "Development of a new Geometric Multi-Grid Finite Element Method and a Semi-Implicit Partitioned Algorithm for Fluid-Structure Interaction Simulation," Ph.D. dissertation, SeoulTech, 2019.
- [12] T. Ryo, B.W. Nigel, H. Nearchos, W.D. Andrew, R.W. Andrew, A.D. Hughes, J. Davies, D.P. Francis, J. Mayet, G.Z. Yang, A.M.T. Simon, X.Y. Xu, "Fluid–structure interaction analysis of a patient-specific right coronary artery with physiological velocity and pressure waveforms," *Commun. Numer. Meth. Engng.*, 25, 2009, pp. 565-580.
- [13] D.R. Einstein, P. Reinhall, M. Nicosia, R.P. Cochran, K. Kunzleman, "Dynamic finite element implementation of nonlinear, anisotropic hyperelastic biological membranes," *Computer Methods in Biomechanics & Biomedical Engineering*, 6.1, pp. 33-44, 2003.
- [14] A. Ranga, R. Mongrain, Y. Biadilah, R. Cartier, "A compliant dynamic FEA model of the aortic valve," *12th IFToMM World Congress, Besançon, France, 2007*, pp. 1-6.
- [15] Y.S. Yu, Y.P. Zhao, "Deformation of PDMS membrane and microcantilever by a water droplet: Comparison between Mooney-Rivlin and linear elastic constitutive models," *Journal of Colloid and Interface Science*, 332.2, pp. 467-476, 2009.

## MÔ PHỎNG SỐ SỰ TƯƠNG TÁC CHẤT LỎNG-CẤU TRÚC CỦA DÒNG MẠCH MÁU VỚI VAN ĐỘNG MẠCH CHỦ BẰNG PHƯƠNG PHÁP PHẦN TỬ HỮU HẠN VÀ CÔNG THỨC ĐƠN KHỐI

**Hà Trường Sang, Vũ Văn Chiên, Nguyễn Mạnh Hùng, Nguyễn Mạnh Đức**

**Tóm tắt:** Bài báo trình bày mô phỏng số sự tương tác giữa chất lỏng và cấu trúc của dòng mạch máu qua van động mạch chủ. Phương pháp rời rạc sử dụng phần tử hữu hạn được áp dụng cho cả hai miền chất lỏng và cấu trúc. Công thức đơn khối được dùng cho sự kết hợp của pha cấu trúc và lỏng nhằm thỏa mãn các điều kiện động học và động lực học tại các biên. Phương pháp tích phân dựa trên lưới di động Euler-Lagrange được áp dụng để giải hệ phương trình Navier-Stokes cho dòng chất lỏng không nén được và công thức tổng hợp Lagrange được dùng cho trạng thái phi tuyến theo mô hình Mooney-Rivlin của van. Phương pháp được kiểm chứng bằng cách so sánh kết quả thu được với các nghiên cứu trước đó cho bài toán truyền áp suất trong ống thẳng ba chiều. Sau đó, phương pháp được sử dụng để mô phỏng dòng mạch máu qua van động mạch chủ. Kết quả mô phỏng số thu được có thể dùng trong việc dự đoán nguy cơ các bệnh về tim mạch...

**Từ khóa:** Tương tác chất lỏng-cấu trúc; phương pháp phần tử hữu hạn; van động mạch chủ; công thức đơn khối.

Received: 21/9/2020; Revised: 21/5/2021; Accepted for publication: 17/9/2021

